Cholesterol homeostasis in hair follicle keratinocytes is disrupted by impaired ABCA5 activity

Megan A. Palmer [a,b,1], Irundika H.K. Dias [c], Eleanor Smart [d,2], Yvonne Benatzy [b], Iain S. Haslam [a,*]

[a] School of Applied Sciences, University of Huddersfield, Huddersfield, UK
[b] Faculty of Medicine, Institute of Biochemistry I, Goethe-University Frankfurt, Frankfurt, Germany
[c] Aston Medical school, Aston University, Birmingham, UK
[d] Centre for Dermatology Research, University of Manchester, UK

ARTICLE INFO

ABSTRACT

The importance of cholesterol in hair follicle biology is underscored by its links to the pathogenesis of alopecias and hair growth disorders. Reports have associated defects in ABCA5, a membrane transporter, with altered keratinocyte cholesterol distribution in individuals with a form of congenital hypertrichosis, yet the biological basis for this defect in hair growth remains unknown. This study aimed to determine the impact of altered ABCA5 activity on hair follicle keratinocyte behaviour. Primary keratinocytes isolated from the outer root sheath of plucked human hair follicles were utilised as a relevant cell model. Following exogenous cholesterol loading, an increase in ABCA5 co-localisation to intracellular organelles was seen. Knockdown of ABCA5 revealed a dysregulation in cholesterol homeostasis, with LXR agonism leading to partial restoration of the homeostatic response. Filipin staining and live BODIPY cholesterol immunofluorescence microscopy revealed a reduction in *endo*-lysosomal cholesterol following ABCA5 knockdown. Analysis of oxysterols showed a significant increase in the fold change of 25-hydroxycholesterol and 7-β-hydroxycholesterol following cholesterol loading in ORS keratinocytes, after ABCA5 knockdown. These data suggest a role for ABCA5 in the intracellular compartmentalisation of free cholesterol in primary hair follicle keratinocytes. The loss of normal homeostatic response, following the delivery of excess cholesterol after ABCA5 knockdown, suggests an impact on LXR-mediated transcriptional activity. The loss of ABCA5 in the hair follicle could lead to impaired *endo*-lysosomal cholesterol transport, impacting pathways known to influence hair growth. This avenue warrants further investigation.

1. Introduction

ABC transporters are a family of membrane proteins responsible for the energy-dependent, active transport of substrates across biological membranes [1]. A little-known member of this family, ABCA5, has yet to be assigned a conclusive function and specific allocrites remain unknown. Some research has suggested a role for ABCA5 in cholesterol transport and/or trafficking, potentially influencing the efflux of cholesterol across the plasma membrane [2,3] or intracellular accumulation within cytosolic compartments [4]. Recently, mutations in ABCA5 were also associated with a form of congenital hypertrichosis [5–7], possibly resulting from alterations in free cholesterol (FC) accumulation within hair follicle (HF) keratinocytes.

The importance of cholesterol in cutaneous physiology is underscored by its essential role in the development and repair of the epidermal permeability barrier [8–10]. Additionally, cholesterol acts as a precursor for the synthesis of local steroid hormones [11,12], plays a role in melanogenisis [13], is involved in corneocyte desquamation [14,15], and influences keratinocyte differentiation [14,16,17]. Furthermore, cholesterol modifications have been associated with numerous signalling pathways which are essential for HF morphogenesis and cycling, such as sonic hedgehog (Shh) [18,19], Wnt/β-catenin

[20] and BMP [21].

Expression of steroidogenic enzymes involved in the synthesis of androgens, oestrogens and glucocorticoids are present in the HF [22]. Most cells furnish their cholesterol needs *via* endogenous biosynthesis; however, in steroidogenic tissues, exogenous sources of cholesterol can be utilised. This can include receptor-mediated endocytosis of lipoprotein cholesterol, often LDL [23]. Alternatively, the bidirectional transporter, scavenger receptor class B member 1 (SCARB1), can facilitate uptake of cholesterol esters from HDL [24]. Such tissues also have the capacity to limit the accumulation of potentially harmful unesterified cholesterol, generally described as FC, by reducing *de novo* biosynthesis, increasing esterification, or increasing active efflux across the cell membrane. This can include efflux by other members of the ABC transporter superfamily, commonly ABCA1 and ABCG1, which transport FC to ApoA1 and HDL, respectively [25–27]. *De novo* cholesterol biosynthesis is tightly regulated through SREBP2 mediated transcription. Small fluctuations in ER cholesterol levels facilitate the transport of the SREBP2 precursor from the ER to the Golgi, where it undergoes proteolytic processing into its mature isoform. Under high cholesterol conditions excess cholesterol is oxidised into oxysterols through both enzymatic and autoxidation, leading to the retention of SREBP2 in the ER through binding of SCAP and INSIG with cholesterol and INSIG, respectively.

We recently reviewed the burgeoning evidence shedding light on the important role for cholesterol in HF biology, noting that maintenance of cholesterol homeostasis is an important process for normal HF morphogenesis, growth and cycling [28]. As such, disruption of cholesterol homeostasis may have a profound impact on HF biology, which could explain the link between ABCA5 mutation and hypertrichosis [5,6].

To further examine the biological role of ABCA5 and the impact of reduced ABCA5 activity, this study examined the homeostatic response of HF derived primary human outer root sheath (ORS) keratinocytes along with *ex vivo* HF culture, to cholesterol loading, before and after ABCA5 knockdown.

2. Materials and methods

2.1. Outer root sheath keratinocyte isolation & culture

ORS keratinocytes were isolated from plucked HFs, obtained from consenting donors. Briefly, cells were incubated in 0.25 % Trypsin-EDTA (Gibco™, Massachusetts, USA) and agitated periodically, as previously described [29–32]. Cells were seeded onto mitomycin C treated human dermal fibroblast feeder layers until confluent. Initial isolation media consisted of DMEM (Sigma-Aldrich, Dorset, UK) 3:1 Ham's F12 (Lonza, Basel, Switzerland) supplemented with 10 % foetal bovine serum (Gibco™), 2 mM L-glutamine, 0.4 μg/ml hydrocortisone (Acros Organics, Geel, Belgium), 5 μg/ml insulin, 2.4 μg/ml adenine (Alfa Aesar™, Massachusetts, USA), 2 nM triiodothyronine (Sigma-Aldrich), 0.1 nM cholera toxin (CTX) (Sigma-Aldrich), 10 ng/ml epidermal growth factor (Sigma-Aldrich), 1 mM ascorbyl-2-phosphate (Sigma-Aldrich), 100 UI/ml penicillin G (Alfa Aesar™) and 25 μg/ml gentamycin (Gibco™). Subculture was achieved through incubation with 1x TrypLE Express (Gibco™) and subsequent growth performed in Epilife media (Gibco™) supplemented with human keratinocyte growth supplement (HKGS) (Gibco™).

2.2. siRNA transfection and cell treatments

Non-targeting (NT) and ABCA5 SMARTpool ON-TARGETplus siRNA (Dharmacon, Horizon, Cambridge, UK) were transfected at 10 nM using Lipofectamine™ RNAiMAX Transfection Reagent (Invitrogen™) in Opti-MEM™ (Gibco™) as per manufactures guidelines. Following incubation with siRNA, cells were treated with 25 μM FC or 10 μM T091317 for 24 h (or appropriate vehicles; 0.5 % ethanol or 0.05 % DMSO respectively). Alternatively, cells were analysed 72 h after initial transfection. Cells for ABCA5 immunocytochemistry were either treated with vehicle or 25 μM FC.

2.3. Immunocytochemistry and fluorescent staining

ORS keratinocytes were seeded onto 13 mm coverslips (Sarstedt) at 67×10^4 cells per ml in 30 μl droplets prior to addition of growth media. Cells were fixed in either Methanol (ABCA5) or 4 % paraformaldehyde (Filipin). For ABCA5 staining in HFs, sections were air dried for 10 min at room temperature and subsequently fixed for 10 min in 100 % Acetone. Non-specific blocking was performed with 10 % normal goat serum (Sigma-Aldrich), and coverslips were incubated overnight at 4 °C with primary antibodies. All primary antibodies were supplied from Abcam; Rabbit anti-ABCA5 1:200 (ab99953), Mouse anti-LAMP1 [H4A3] 1:200 (ab25630), Mouse anti-PDI [RL90] 1:200 (ab2792), Mouse anti-ATBP [3D5] 1:1000 (ab14730). Secondary antibodies, Goat-anti-Rabbit Alexa Fluor® 594 (A11012, Invitrogen™) and Goat-anti-Mouse Alexa Fluor® 488 (A11001, Invitrogen™) were incubated for 45 min at room temperature at 1:200 dilutions (or 1:500 for PDI). Filipin (Sigma-Aldrich) staining for FC was performed following fixation in 4 % paraformaldehyde (PFA) for 10-minutes, quenched with 10 mg/ml glycine (Fisher); Filipin was added at 100 μg/ml in 1× PBS with 10 % FBS for 2 h at room temperature. Counterstaining (for ABCA5) was performed for 1 min with 1 μg/ml 4′,6-diamidino-2-phenylindole (DAPI; Sigma-Aldrich). MemGlow™ NR12A membrane polarity probe (Cytoskeleton, Inc.) staining was performed at 20 nM for 10 min at room temperature.

2.4. Preparation of BODIPY-cholesterol

BODIPY-cholesterol (TopFluor® Cholesterol; Avanti lipids, Alabama, USA) was prepared by complexing at a molar ratio of 1:10 with 25 mM Methyl-β-cyclodextrin. This stock solution was sonicated in a water bath at 37 °C for 30-minutes, then placed into an orbital shaker for 2 h, and stored at −20 °C. Immediately prior to use BODIPY-cholesterol solution was sonicated in a water bath at 37 °C for 30-minutes, then a working solution of 25 μM was prepared in HBSS-HEPES.

2.5. Live cholesterol staining

Cells were seeded into micro-Insert 4 Well in 35 mm μ-Dish with ibidi treat polymer coverslips (ibidi, Planegg, Germany) at 2×10^4 cells per ml and incubated overnight. Following transfection, cells were washed once in HBBS-HEPES and then incubated first with ER Staining Kit - Red Fluorescence - Cytopainter (ab139482; abcam) at 1:500 for 15 min, followed by Mitochondrial Staining Reagent - Blue - Cytopainter (ab219940; abcam) at 1:500 and LysoTracker™ Deep Red (L12492; Invitrogen™) at 1:20,000 for 30 min. Immediately prior to imaging cells were incubated with 25 μM BODIPY-cholesterol.

2.6. Masson's Fontana

Silver nitrate stock solution was prepared using 10 % silver nitrate (Honeywell, North Carolina, USA) in distilled water, ammonium hydroxide (Fisher) was added dropwise until the solution turned brown and back to clear again. The stock solution was left in the dark for 24-hours to develop. The working solution was used at 1:4 dilution in distilled water. Slides were air-dried for 10-minutes, then fixed in a 2:1 ethanol: glacial acetic acid mixture for 10-minutes. Slides were placed into silver nitrate working solution and microwaved for 2–3-minutes, followed by incubation with 5 % sodium thiosulfate (Fisher) solution for 1-minute. Counter staining with Mayer's Haematoxylin (Sigma-Aldrich) was performed for 2-minutes. Brightfield images were acquired with Axio observer Z1/7 microscope (Zeiss, Oberkochen, Germany). Images were analysed using ImageJ Fiji, by converting to 8-bit, then inverting

grayscale. Epithelial components of the bulb were outlined using the polygon line tool and mean pixel intensity was measured.

2.7. Ki67-TUNEL staining

Tissue sections were air-dried for 10-minutes, and fixed with ethanol-glacial acetic acid (2:1) for 5-minutes. Click-iT™ Plus TUNEL Assay Kits for *In Situ* Apoptosis Detection (C10619; Invitrogen™) was utilised as per manufacturer's instructions to detect apoptosis *via* TUNEL (terminal deoxynucleotidyl transferase dUTP nick end labelling). Following TUNEL staining, slides were washed with PBS, blocked in 10 % NGS for 20-minutes and incubated with primary Rabbit anti-Ki67 antibody [SP6] (ab16667) at 1:200 dilution in 2 % NGS in a humidified chamber at 4 °C overnight. Following washes with PBS, sections were incubated with Alexa Fluor Goat anti-rabbit IgG 555 (H + L) Cross-Adsorbed Secondary Antibody (Invitrogen™) was incubated for 45-minutes at room temperature in a 1:200 dilution in 2 % NGS. Subsequent washed in PBS and counterstaining with DAPI at 1 μg/ml was performed.

2.8. Microscopy

Confocal microscopy was performed using either a Zeiss laser scanning microscope 880 or 800 Axio-Observer using Zen Black v2.3 software for acquisition (or Zen blue for 800). Images were acquired with Plan-Apochromat 40×/1.4 Oil DIC M27 objective. Airyscan processing was performed using Zen software.

For live cell imaging, images were acquired with a LD LCI Plan-ApochromatAprochromat 40×/1.2 Imm Korr IC M27 objective with a Z-stage Piezo and glycerol immersion using fast Airyscan. Z-stack settings for 20 μm from the centre were optimised for complete coverage of all 4 regions and allowed for changes in Z position over time. Six time points were acquired over a period of 3 h. Image registration was performed using Zen Blue to correct for Z-drift. Images were split into separate time points subsequent to image analysis.

For tissue sections, images were acquired with an Axio obsever Z1/7 microscope (Zeiss) using a Plan-Apochromat 63×/1.4 Oil DIC M27 with objective AxioCam 305 mono camera or with Vectra Polaris (Akoya Biosciences) using the 20× objective.

2.9. Flow cytometry

CTX-FITC (Sigma-Aldrich) was reconstituted at 2.5 mg/ml stock in water. Cells were seeded at 10×10^4 per ml in 24 well plates prior to siRNA transfection. Cells were washed twice in ice cold PBS and then fixed with 1 % PFA (w/v) for 5-minutes on ice. Following fixation cells were washed twice in ice-cold PBS containing 3 % BSA, then incubated with 6 μg/ml CTX-FITC (Sigma-Aldrich) for 30 min at room temperature. Two more washes in ice-cold PBS with BSA were performed before cells were scraped in ice-cold PBS. Flow cytometry analysis was performed using a Guava® easyCyte™ SL 5 flow cytometer (Merck).

Streptolysin O was reconstituted at 14.5 mM in dithiothreitol (DTT), diluted to a working solution of 29 nM in media containing 5 μg/ml propidium iodide (PI) and incubated for 1 h. Cells were subsequently washed 2× with PBS and then isolated with TrypLE. Following centrifugation cells were resuspended in FACS flow. Flow cytometry was performed using a FACS Symphony A5 (BD biosciences). Gating was determined in FlowJo using PI and DTT + PI treated negative controls.

2.10. Protein extraction

Cells were seeded at 4×10^4 cells per cm^2 into three wells of a 6 well plate and scraped in ice-cold PBS. Both nuclear and membrane protein extracts were isolated using Nuclear Extraction kit (ab113474; abcam) as per manufacturers' instructions. Membrane fractions were supplemented with additional SDS to a final volume of 0.1 %. Cell lysates were

sonicated for 30 s using a probe sonicator.

2.11. Western blotting

40 μg of total protein was loaded into NuPage™ 3–8 % tris acetate gels (Invitrogen™) and run for 1 h at 150 V. Transfer was performed on iBlot2 (Invitrogen™) using PVDF membrane transfer stacks (Invitrogen™) for 10 min. Membranes were incubated in Intercept® TBS blocking buffer (Licor®, Nebraska, USA) for 1 h and primary antibodies were incubated overnight at 4 °C on a rocker. ABCA1 (ab18180, abcam), ABCA5 (ab99953, abcam), ABCG1 (ab52617, abcam) (1:500), SCARB1 (1:1000; ab217318, abcam), containing β-Actin (1:40000; rabbit ab8227, abcam or mouse MAB1501, Millipore Limited, Hertfordshire, UK). Membranes were washed with TBS-T then incubated with secondary antibodies at 1:1000 dilution, Goat-anti-mouse Alexafluor 790 (Invitrogen™) or Goat-anti-rabbit Alexafluor 690 (Invitrogen™) for 1 h at room temperature. Membranes were imaged using Odyssey imaging system (Licor®). Densitometry was performed using image studio lite (Licor®).

2.12. SREBP2 transcription factor activity assay

Nuclear fractions were thawed and immediately used for the assay with 30 μg of protein per reaction. SREBP2 assay was measured *via* ELISA method as per manufacturers' instructions using SREBP2 transcription factor assay kit (abcam; ab133111). Absorbance was measured at 450 nm on a BMG Labtech SPECTROstar Nano.

2.13. Cholesterol efflux assay

ORS keratinocytes were seeded at 2×10^4 per well in 48 well plates and transfected for 72 h as described above. Cells were washed in Epilife prior to incubation with 25 μM BODIPY-cholesterol. Cells were washed in Epilife and equilibrated for 24 h with Acyl-CoA:cholesterol acyltransferase (ACAT) inhibitor, 2 μg/ml Sandoz 58-035 (Sigma-Aldrich) for 22 h. Cells were washed in a 10 mM HBSS-HEPES solution (Lonza) and efflux was initiated by adding cholesterol acceptors, 10 μg/ml ApoA1 (Sigma-Aldrich) or 25 μg/ml HDL (Sigma-Aldrich) for 4 h. Background efflux was performed in the absence of cholesterol acceptors. Media was removed and fluorescence measurements performed in black-walled 96 well plates (excitation 485/20 nm, emission 528/20 nm).

2.14. Gene expression analysis

ORS keratinocytes were seeded into 12 well plates at 20×10^4 cells per well and cultured overnight. Following transfection (as described above) cells were incubated with either 25 μM FC (or 0.025 % ethanol vehicle control) or 5 μM T0901317 (or 0.05 % DMSO vehicle control) (Sigma-Aldrich) for 24 h. ORS keratinocytes were pelleted prior to RNA extraction. RNA extraction was performed using Relia prep (Promega, Wisconsin, United States) according to manufacturer's instructions. cDNA synthesis was achieved using Tetro cDNA synthesis kit (Bioline, London, UK) converting 100–1000 ng of RNA. qPCR was performed using TaqMan™ gene expression assays (Applied biosciences™, Massachusetts, USA) and Precision Fast mastermix (Primerdesign, Southampton, UK) with a StepOne plus instrument (Applied biosciences™). Analysis was performed using ΔΔCT method. Taqman assay IDs: ABCA1; Hs01059118_m1, ABCA5; Hs00363322_m1, ABCG1; Hs00245154_m1, PPIA; Hs99999904_m1, HMGCR; Hs00168352_m1, SCARB1; Hs00969821_m1, SREBP2; Hs01081784_m1.

2.15. Lipidomic analysis

Cells were seeded at 4×10^4 per cm^2 in three wells of a 6 well plate subsequent to transfection (as described above). After 48 h incubation

25 μM FC (or 0.25 % ethanol vehicle control) was added for 24 h. Cells were lysed using 1xTrypLE for 10-minutes and centrifuged at 200g for 8 min. Supernatant was removed and pellets were immediately snap-frozen on dry ice and stored in −80 °C until further analysis. Oxysterols were extracted from cell pellets spiked with 1 ng of deuterated internal standards (24-OHCd7, 25-OHCd6, 27-OHCd6, 7β-OHCd7 and 7-KCd7). Briefly, cell pellets were resuspended in 50 μl water and mixed with 450 μl methanol containing 50 μg/ml BHT, vortexed for 30 s and sonicated for 10 min before centrifugation at 14,000 ×g for 10 min. The methanolic supernatant was collected and dried under a vacuum.

The lipid extracts were dissolved in 100 μl of 40:60 Methanol: H2O and analysed with a liquid chromatography UltiMate 3000 HPLC system (Dionex, Thermo Scientific Ltd.) coupled on-line with an electrospray tandem triple quadrupole-linear ion trap mass spectrometer (QTrap 5500, ABSciex) as described previously (Dias et al., 2018).

2.16. Hair follicle organ culture

Temporal scalp skin was obtained *via* surplus material from face lift surgeries (Caltag Medsystems Ltd., Buckingham, UK). Tissue was obtained with informed consent and storage was in accordance with the Human Tissue Act 2004 in the Huddersfield Skin & Hair Biobank. HFs were cultured in accordance to [33–35] in Williams E medium (Gibco™) supplemented with 1 % penicillin-streptomycin, 1 % L-glutamine, 10 μg/ml insulin and 10 ng/ml hydrocortisone. Prior to treatment HFs were incubated overnight to acclimatise. The following day the media was replaced with fresh HF media containing either 25 μM FC and incubated for 24-hours, 5 mM MβCD and incubated for 1-hour with 23-hours recovery time, or incubated for 72-hours with Accell Human ABCA5 siRNA (E-004345-00-0005; Horizon discovery) or Accell Non-Targeting control pool (D-001910-10-05), followed by 24-hours with 25 μM FC or vehicle control. Following treatment HFs were snap frozen in Richard-Allan Scientific™ Neg-50™ Frozen Section Medium (Thermo Scientific™) and cryosectioned at 7 μm thickness.

2.17. Image analysis

To determine the co-localisation of either ABCA5, filipin or BODIPY-cholesterol to intracellular markers, ImageJ FIJI [36] was used. Macros were written to determine the mean pixel intensity within the masked area of the organelle *via* Otsu thresholding. NR12A images were analysed for intensity per cell and the ratio was generated by dividing the intensity of Lo (550–600 nm) by Ld (600–650 nm). Ratiometric images were generated using RatioIoJ plugin developed by Romain Vauchelles [37]. For HFs, manual annotations were performed in QuPath v0.4.2 [38] and mean pixel intensities of whole follicles for ABCA5 were utilised. Stardist plugin [39] for qupath was utilised to detect positive nuclei in Ki67 TUNEL images using a threshold value of 8 and 25 for Ki67 and TUNEL respectively. Masson Fontana analysis was performed in ImageJ FIJI, converting images to 8-bit and inverting before measuring mean pixel intensity. 10 images with a minimum of 90 cells per donor were analysed. For live imaging 2 images containing.

2.18. Statistical analysis

Statistical analysis was performed using Prism (GraphPad, California, USA). Normality testing *via* Shapiro-Wilk testing was performed prior to two-tailed, one-sample *t*-tests, unpaired t-tests or one-way ANOVA with Dunnett's comparisons, as appropriate. Statistical significance was described as * $P \leq 0.05$, ** $P \leq 0.01$, *** $P \leq 0.001$.

3. Results

3.1. Exogenous cholesterol loading alters ABCA5 co-localisation with intracellular organelles

Firstly, the intracellular localisation of ABCA5 was examined by immunofluorescence co-localisation with intracellular organelle markers for *endo*-lysosomes (lysosomal associated membrane protein 1; LAMP1), ER (protein disulfide isomerases; PDI) and mitochondria (ATP synthase subunit beta; ATPB). Fig. 1 shows moderate co-localisation of ABCA5 to intracellular organelles. Following 72-hours FC exposure, a significant increase in ABCA5 co-localisation with PDI was observed (2.7-fold; $P < 0.05$). A 2.8-fold increase in mean pixel intensity for total ABCA5 protein was also seen ($P = 0.053$). This was confirmed by western blot analysis (Fig. 1C) where a 3.2-fold change in the 400 kDa oligomeric isoform of ABCA5 was found following cholesterol loading. ABCA5 protein detected by western blotting also revealed isoforms at 99, 187 and ~300 kDa; no change in these isoforms was observed with the addition of FC. Neither LXR activation [40] nor FC loading increased ABCA5 mRNA expression (Fig. S1).

3.2. ABCA5 knockdown alters cholesterol distribution following loading

Next, to help establish the role of ABCA5 in cholesterol compartmentalisation, an ABCA5 knockdown was established in ORS keratinocytes. A 79 % reduction in mRNA was achieved 24 h after treatment with siRNA (Fig. 2A). Analysis of ABCA5 immunofluorescence (Fig. 2B) revealed a 22 % reduction in mean ABCA5 pixel intensity (Fig. 2C). By Western blot (Fig. 2D), a 50 % reduction in the oligomeric 400 kDa isoform ($P = 0.062$) and a 70 % reduction in the 99 kDa ABCA5 protein was observed (Fig. 2E).

The cellular response to exogenous cholesterol loading was examined following ABCA5 knockdown. ORS keratinocytes were exposed to 25 μM FC in the presence or absence of ABCA5 knockdown. Changes in FC distribution were examined by filipin staining (Fig. 3A) Excess intracellular cholesterol can accumulate in the lysosome for transport to the PM for efflux, or alternatively be converted into oxysterols *via* autoxidation or through enzymes located in the ER or Mitochondria. Furthermore, small fluctuations in cholesterol at the ER alters SREBP2 signalling [41], therefore these organelles were chosen to investigate cholesterol distribution.

In the absence of ABCA5 knockdown, FC loading led to a significant increase in total (Fig. 3E) and *endo*-lysosomal cholesterol (Fig. 3B), as shown by the increased co-localisation with LAMP1 (Fig. 3A). Knockdown of ABCA5 did not alter FC distribution in the absence of exogenous cholesterol loading. By contrast, ABCA5 knockdown substantially decreased the FC loading induced endo-lysosomal cholesterol ($P = 0.062$ Fig. 3B). Mitochondrial cholesterol was significantly reduced by the addition of FC, with no impact of ABCA5 knockdown observed (Fig. 3D).

In order to assess plasma membrane cholesterol levels three techniques were employed: membrane polarity probe NR12A, Streptolysin O pore formation and detection of lipid rafts with cholera toxin (CTX). NR12A exhibits a 50 nm spectral shift from lipid ordered (Lo) compared to lipid disorder (Ld). Danylchuk et al. [42] demonstrated small changes in the 550–600/600–650 (Lo/Ld) ratio of cells enriched or depleted of cholesterol. FC treatment alone increased the Lo/Ld ratio from 1.469 to 1.472, a further increase to 1.538 was observed in ABCA5 knockdown cells. In contrast, ABCA5 knockdown cells treated with FC revealed a subtle decrease in Lo/Ld ratio from 1.538 to 1.519 (Fig. 4A+B).

Streptolysin O is a cholesterol-dependant cytolysin produced by *Streptococcus pyogenes* which forms pores in the plasma membrane. When utilised in conjunction with PI, which is normally in unable to penetrate live intact cells, SLO can indicate alterations in plasma membrane cholesterol [43]. Flow cytometry analysis (Fig. 4C) revealed a 2.208 fold change in PI in NT siRNA cells treated with FC. Likewise, a 2.169 fold change was detected in ABCA5 knockdown cells, indicating
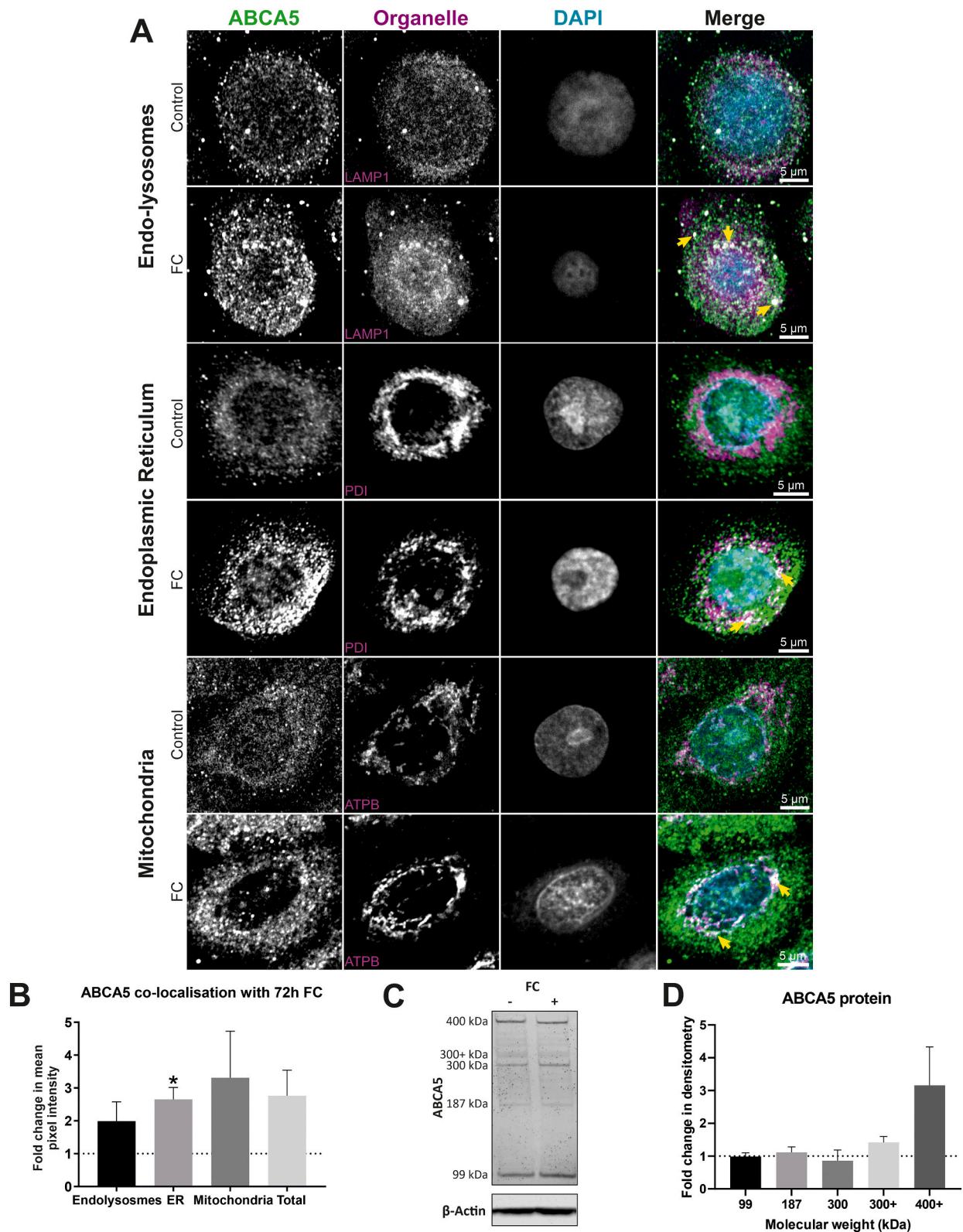
Fig. 1. ABCA5 co-localises to intracellular organelles with free cholesterol treatment in outer root sheath keratinocytes. (A) Dual immunocytochemistry staining of ABCA5 (green) with *endo*-lysosomal marker LAMP1 (magenta), ER marker PDI (magenta) and mitochondrial marker ATPB (magenta) in ORS keratinocytes treated with 25 μM FC or 0.5 % ethanol vehicle control for 72 h. Counterstained with DAPI (cyan), yellow arrows represent co-localisation of ABCA5 when treated with FC to endo-lysosomes, ER and mitochondria. Scale bars represent 5 μm. (B) Image analysis for fold change in mean pixel intensity masked to organelle marker or total pixel intensity. Data are mean ± SEM for $N = 3$ or 9 (total), 5 images per donor (total 93–102 cells per treatment). One-sample *t*-test performed; significance denoted by * $P \leq 0.05$. (C) Western blotting of ABCA5 in ORS keratinocytes treated with 25 μM FC or 0.5 % ethanol vehicle control for 72 h. (D) Protein densitometry values relative to reference protein β-Actin. Data are mean ± SEM for $N = 5/4$ donors.
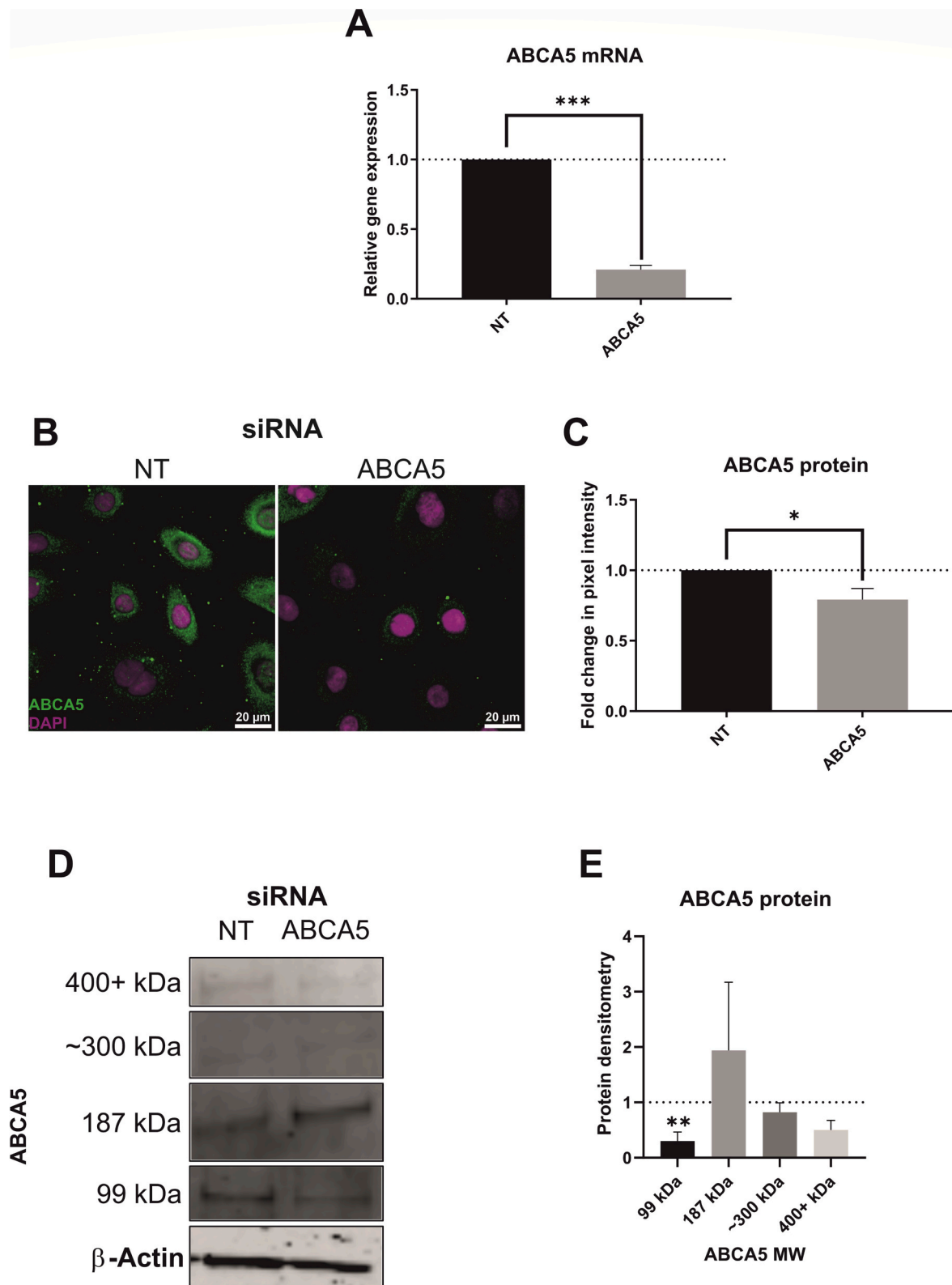
Fig. 2. ABCA5 mRNA and protein levels are significantly reduced with siRNA. (A) ABCA5 gene expression changes in ORS keratinocytes transfected with NT or ABCA5 siRNA for 24 h show a significant reduction in mRNA. Gene expression relative to NT and normalised to PPIA. (B) ABCA5 immunocytochemistry staining (green) in ORS keratinocytes transfected with NT control or ABCA5 siRNA for 72 h. Scale bars 20 μm, counterstained with DAPI (magenta) for nuclei. (C) Fold change in mean pixel intensity per cell of ABCA5 immunocytochemistry staining (Total of 3114 and 2756 cells per treatment). (D) Western blot for ABCA5 in ORS keratinocytes transfected with NT or ABCA5 siRNA for 72 h. (E) Protein densitometry values relative to reference protein β-Actin. Data are mean ± SEM for $N = 4$ donors. One sample t-test performed; significance denoted by * $P < 0.05$, ** $P < 0.01$, *** $P < 0.005$.
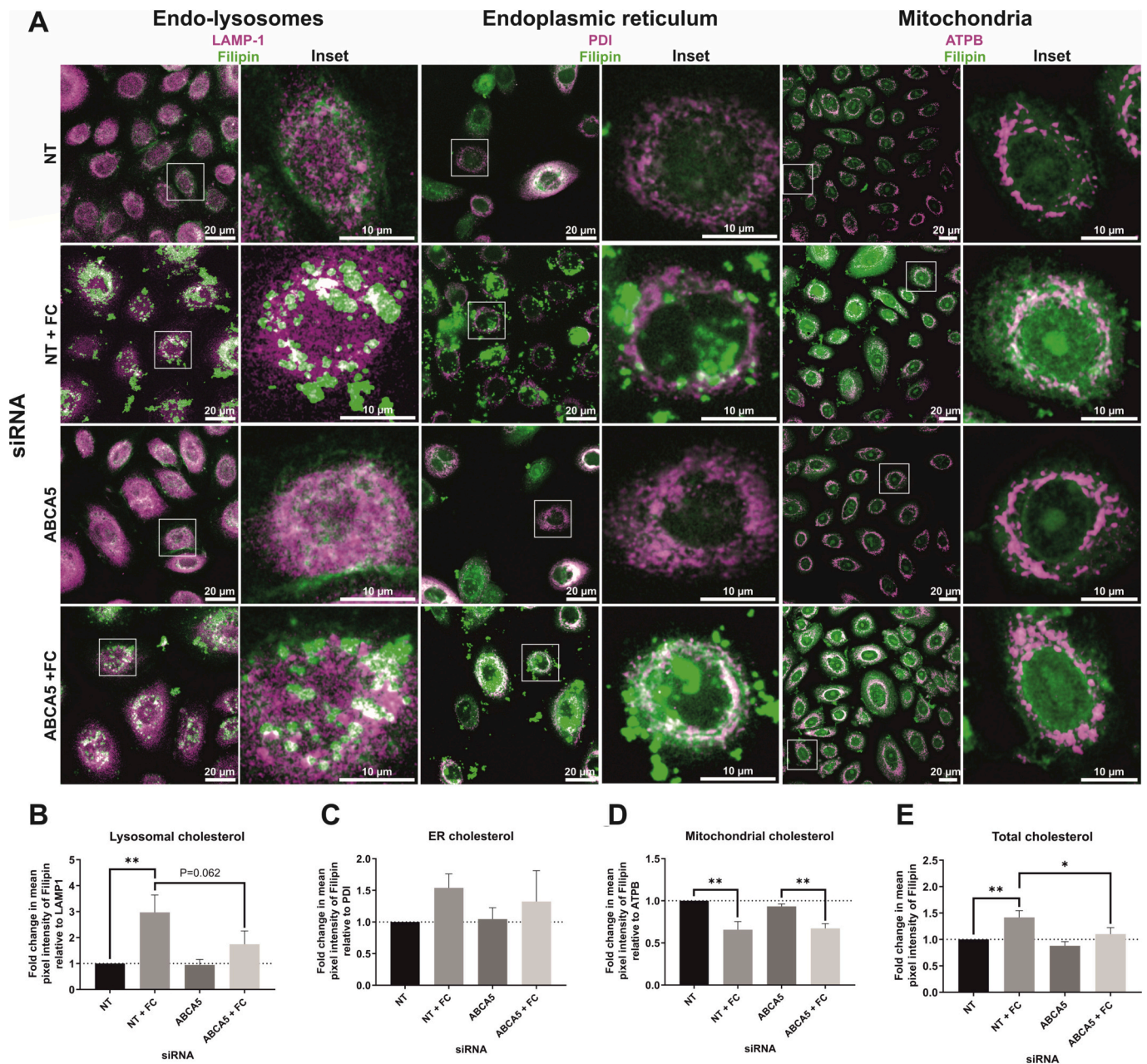
Fig. 3. ABCA5 knockdown alters endo-lysosomal cholesterol. Filipin staining (green) in ORS keratinocytes cells transfected with NT or ABCA5 siRNA for 48 h, with the addition of 25 μM FC or 0.5 % ethanol vehicle control for 24 h. Dual immunocytochemistry staining was performed (magenta) with antibodies for LAMP1 (A), PDI (B) and ATPB (C). Scale bars represent 20 μm. Image analysis of fold change in mean pixel intensity masked to organelle marker (D–F) or total pixel intensity per cell (G). Data are mean ± SEM from 10 images (209–223 cells per treatment) for $N = 4/5$ donors, total $N = 13$. One-way ANOVA were performed with Fisher's multiple comparisons test; significance denoted by * $P \leq 0.05$, ** $P \leq 0.01$, *** $P \leq 0.005$.

higher levels of cholesterol in the plasma membrane. In conjunction with the NR12A data, FC treated ABCA5 knockdown cells had a significantly reduced fold change in PI fluorescent intensity in comparison to both ABCA5 knockdown cells and NT siRNA FC treated cells.

Assessment of CTX-FITC fluorescence (Fig. 4D) showed no changes in lipid raft cholesterol following ABCA5 knockdown or exogenous cholesterol loading.

3.3. Endo-lysosomal BODIPY-cholesterol accumulation is reduced by ABCA5 knockdown

Next, live cell imaging using BODIPY-cholesterol was utilised to determine real-time cellular cholesterol distribution following

exogenous loading. BODIPY-cholesterol (25 μM) was complexed 1:10 with methyl-β-cyclodextrin to enable a rapid uptake of cholesterol for live cell tracking, as previously reported by Holtta-Vuori et al. [44]. As shown in Fig. 5A, which shows a time-lapse of 150-minutes with 30-minute intervals, after entering the cell, cholesterol accumulates intracellularly, increasing in intensity over time. Dual staining with organelle markers for *endo*-lysosomes, ER and mitochondria were performed in tandem with the BODIPY-cholesterol loading. Cholesterol co-localisation with all three markers increased substantially over time. Endo-lysosomal accumulation was significantly reduced by ABCA5 knockdown at 30, 90, 120 and 150-minutes ($P = 0.035$, 0.044, 0.034, 0.048, respectively) (Fig. 5B). This confirms the changes detected with filipin staining (Fig. 3B). No changes were observed for cholesterol
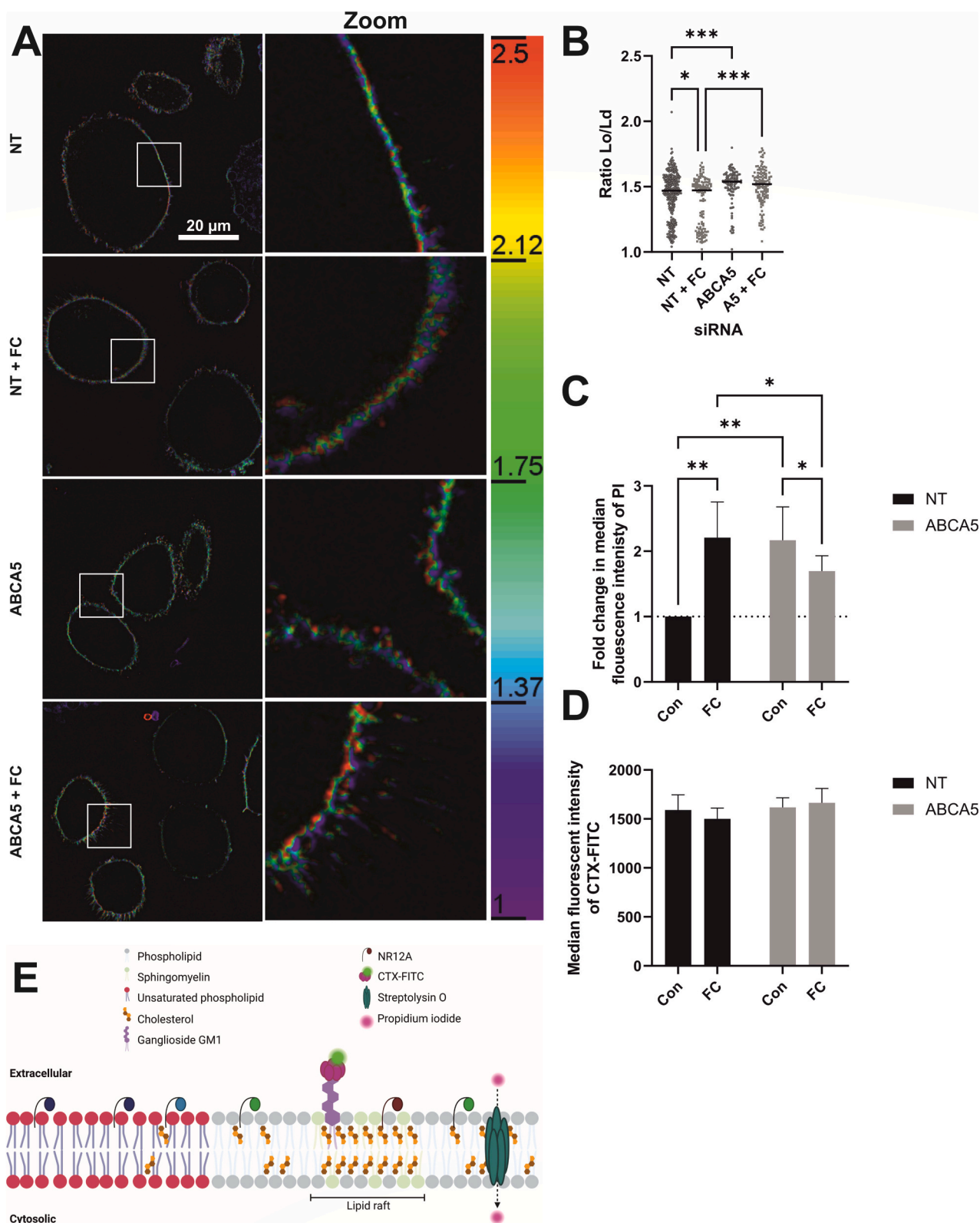
Fig. 4. Membrane lipids with ABCA5 knockdown. Analysis of membrane lipids in ORS keratinocytes transfected with NT or ABCA5 siRNA for 48 h, with the addition of 25 μM FC or 0.5 % ethanol vehicle control for 24 h *via* confocal microscopy NR12A (A,B) or flow cytometry of propidium iodide following streptolysin O mediated pore formation (C) or CTX-FITC (D). (E) Representative figure created in Biorender of biochemical techniques utilised to measure membrane lipids. NR12A shows a 50 nm spectral shift in lipid order *vs* lipid disordered domains (represented by blue to red colour change). Streptolysin O binds to the accessible cholesterol pool in the plasma membrane forming pores and allowing the transport of propidium iodide into the cell. CTX conjugated with FITC binds to ganglioside GM1 representing the lipid raft pool of cholesterol. Data are median ± SEM $N = 3$–4 donors, One-way ANOVA performed, significance denoted by * $P \leq 0.05$, ** $P \leq 0.01$, *** $P \leq 0.005$ For NR12A 105–135 cells were analysed per treatment.
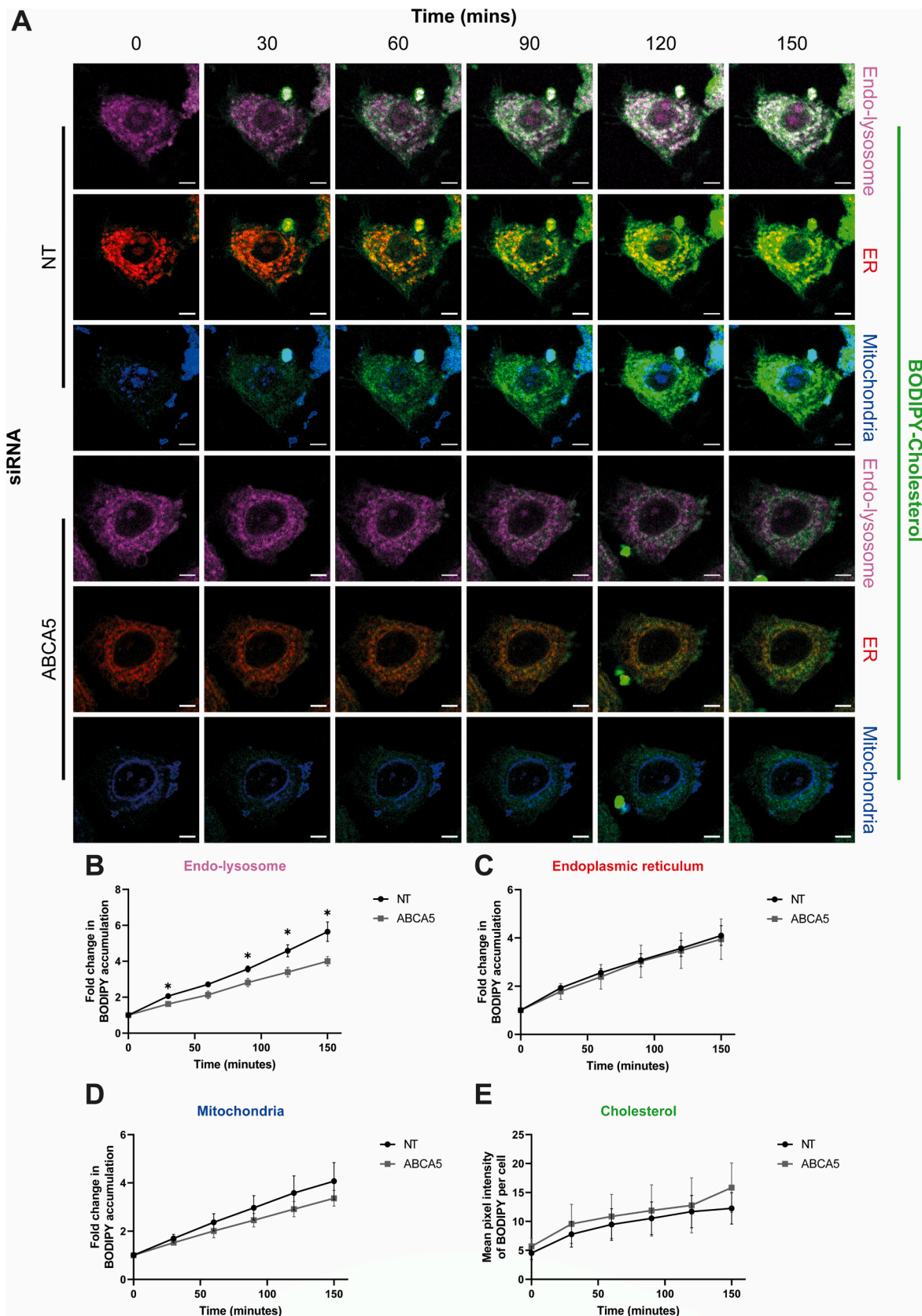
Fig. 5. Endo-lysosomal cholesterol accumulation is significantly reduced in ABCA5 knockdown outer root sheath keratinocytes. (A) ORS keratinocytes cells transfected with NT or ABCA5 siRNA for 48 h incubated with 25 μM of BODIPY cholesterol (green), LysoTracker (magenta), ER Cytopainter (red), Mitochondria Cytopainter (blue). Time-lapse images taken at 30-minute intervals for 150-minutes. Scale bars 5 μm. Quantification of mean peak intensities of BODIPY cholesterol masked to organelle marker (B–D) or total (E) per cell. Data are mean ± SEM from 2 images per $N = 4$ donors, containing a total of 200/209 cells (NT/ABCA5). Two-way ANOVA performed with Fisher's multiple comparisons test; significance denoted by * $P \leq 0.05$.

accumulation within the ER or mitochondria (Fig. 5C and D). ABCA5 siRNA knockdown had no impact on the total accumulation of BODIPY-cholesterol (Fig. 5E).

3.4. ABCA5 knockdown impedes cholesterol efflux to ApoA1 through reduction in ABCA1

To investigate the influence of ABCA5 activity on the extrusion of cholesterol across the plasma membrane, BODIPY-cholesterol efflux assays were performed following ABCA5 knockdown. The two primary pathways for the efflux of intracellular cholesterol are ABCA1 and ABCG1-mediated efflux, both of which are expressed in keratinocytes of the epidermis and HF [45–47]. ABCA1 and ABCG1 move cholesterol to the acceptor molecules ApoA1 and HDL, respectively [48,49]. Efflux to HDL was much greater (~13 %) than to ApoA1 (~8 %) in the NT cells. Following ABCA5 knockdown, no change in efflux to HDL was observed (Fig. 6C). Conversely, a significant drop in ABCA1-mediated efflux to

ApoA1 was seen (Fig. 6D).

To investigate the reduction in cholesterol efflux to ApoA1, western blot analysis was performed for ABCA1, ABCG1 and SCARB1, to understand whether reduction of the expression of cholesterol efflux proteins occurred as a result of ABCA5 knockdown (Fig. 6A, B). No significant changes were detected for SCARB1, with a non-significant increase in ABCG1 protein observed. A non-significant reduction in ABCA1 protein was also seen ($P = 0.055$). These results prompted further investigation into whether cholesterol homeostatic pathways may be more broadly disrupted by ABCA5 knockdown.

3.5. ABCA5 knockdown disrupts the homeostatic response to exogenous cholesterol in outer root sheath keratinocytes

Delivery of exogenous cholesterol elicits a cellular homeostatic response, generally through the activation or repression of lipid sensitive transcription factors. Excess cellular cholesterol can be converted
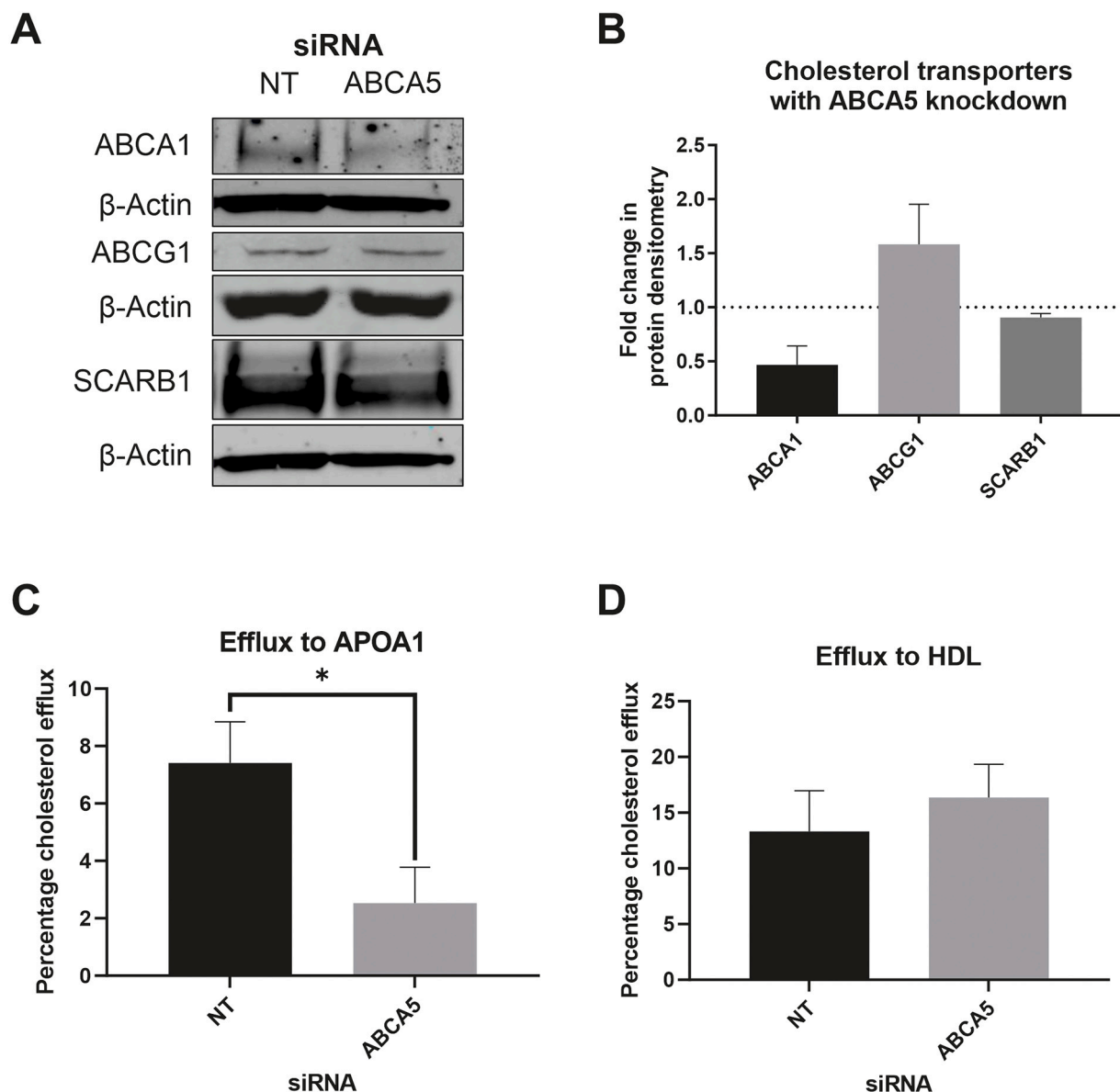

Fig. 6. ABCA5 knockdown reduced cholesterol efflux to ApoA1. (A) Protein expression of ABCA1, ABCG1 and SCARB1 in ORS keratinocytes cells transfected with NT or ABCA5 siRNA for 72 h. Protein densitometry values relative to reference protein β-Actin. Data are mean ± SEM for N = 4 donors. BODIPY cholesterol efflux in ORS keratinocytes cells transfected with NT or ABCA5 siRNA for 72 h. Efflux to ApoA1 (C) or HDL (D). Data are mean percentage change in efflux ± SEM *N* = 6 (C) N = 3 (D) donors. Unpaired *t*-test performed; significance denoted by * P ≤ 0.05.

into oxysterols, which in turn activate LXR leading to an increase in transcription of ABC transporters associated with sterol efflux [26]. SREBP2 is associated with the transcription of genes involved in *de novo* cholesterol biosynthesis [26,27]; binding of cholesterol to SCAP and oxysterols to INSIG results in the retention of SREBP2 in the ER, preventing transportation to the Golgi, where SREBP2 would undergo proteolytic cleavage to form the mature transcription factor [26].

Addition of 25 μM exogenous cholesterol to ORS keratinocytes increased the expression of genes responsible for cholesterol efflux (ABCA1, ABCG1 and SCARB1) with no change in ABCA5 expression (Fig. 7). However, expression of HMGCR, the gene encoding the rate-limiting enzyme in cholesterol biosynthesis, was reduced (Fig. 7I). Knockdown of ABCA5 did not significantly alter the expression of ABCA1, ABCG1, SCARB1 or HMGCR. Strikingly, ABCA5 knockdown lowered the FC-mediated increases in ABCA1 and ABCG1 (Fig. 7B, C). Furthermore, HMCGR was downregulated to a much greater degree following addition of FC to the ABCA5 knockdown cells (Fig. 7I).

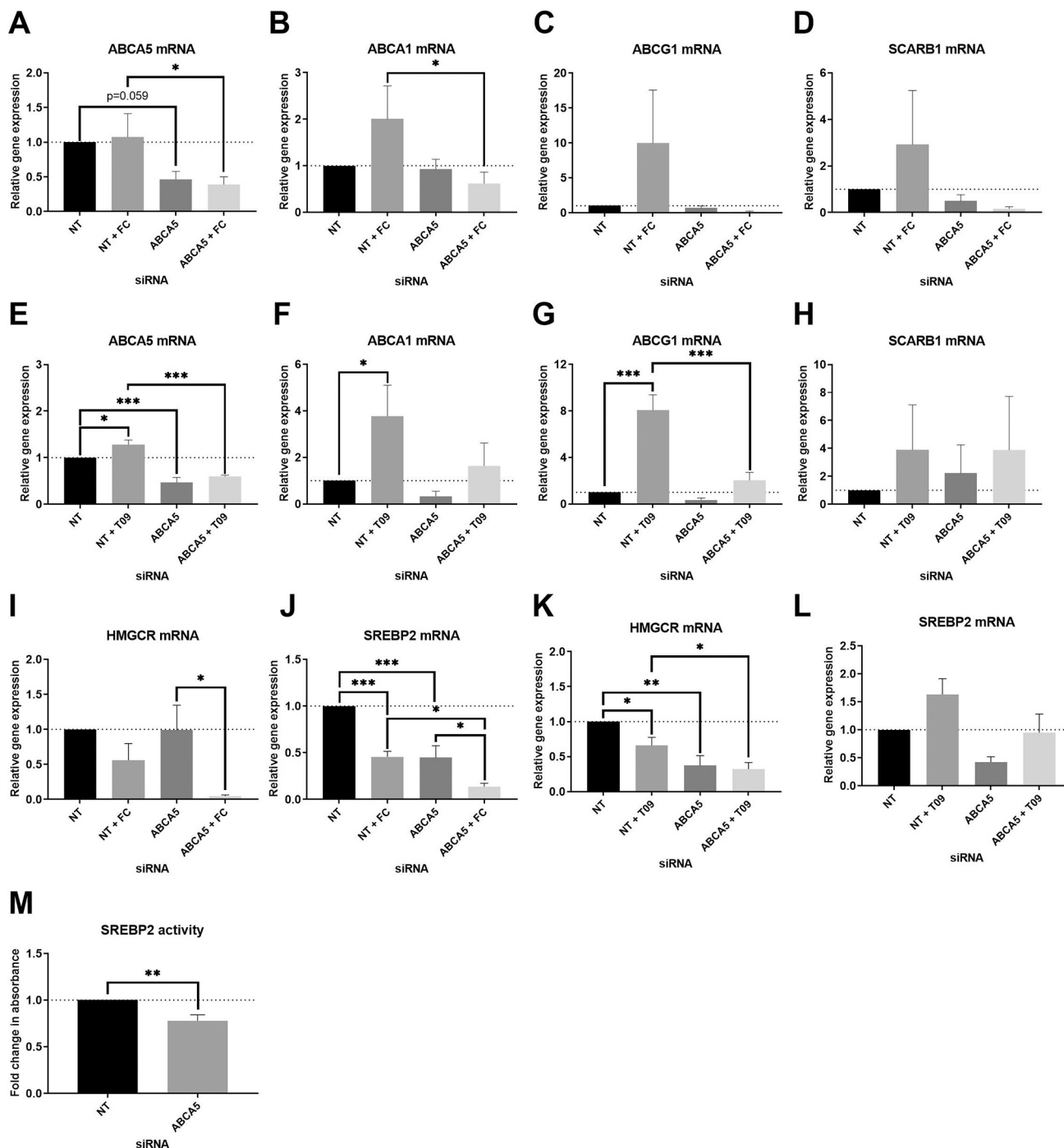These data suggested that the homeostatic response to FC loading

Fig. 7. ABCA5 knockdown disrupts cholesterol homeostasis. Gene expression changes in ORS keratinocytes transfected with NT or ABCA5 siRNA for 48 h, with 25 μM FC or 0.5 % ethanol vehicle control (A-D,I-J), or 5 μM T0901317 or 0.05 % DMSO vehicle control (*E*-H,K-L) for a further 24 h. Gene expression reported relative to vehicle control and normalised to PPIA. Data are mean ± SEM for $N = 5/N = 3$ (FC/T0901317). One-way ANOVA were performed with Fisher's multiple comparisons test; significance denoted by * $P \leq 0.05$, ** $P \leq 0.01$, *** $P \leq 0.005$. (M) Transcriptional activity of SREBP2 in ORS keratinocytes transfected with NT or ABCA5 siRNA for 72 h. Data are mean ± SEM for N = 4 donors. Unpaired t-test performed; significance denoted by ** $P \leq 0.01$.

was altered. To determine whether this was the result of impaired LXR activation, ORS keratinocytes were treated with the agonist T0901317. In the absence of ABCA5 knockdown, LXR activation significantly increased ABCA1 and ABCG1 expression, with a small reduction in HMGCR (Fig. 7F, G, K). As HMGCR is primarily be regulated by activation of SREBP2, a significant reduction in expression may not be expected following LXR activation. Importantly, T0901317 addition to ABCA5 knockdown ORS keratinocytes continued to elicit the typical LXR response, namely ABCA1 and ABCG1 were increased in comparison to ABCA5 knockdown alone, with no significant differences noted in control cells (Fig. 7F, G). This is in sharp contrast to the addition of FC,

which could not induce ABCA1 and ABCG1 expression in the ABCA5 knockdown cells (Fig. 7B, C).

Further analysis demonstrated that SREBP2 transcription was significantly reduced by 22.1 % following ABCA5 knockdown (Fig. 7M). Loading with FC reduced SREBP2 mRNA, which was reduced to a much greater degree in ABCA5 knockdown ORS keratinocytes following FC loading (Fig. 7J). This may account for the extreme reduction in HMGCR mRNA levels detected in FC-loaded ABCA5 knockdown ORS keratinocytes.

Furthermore, although there were no changes to either total or intracellular cholesterol levels following knockdown of ABCA5, a
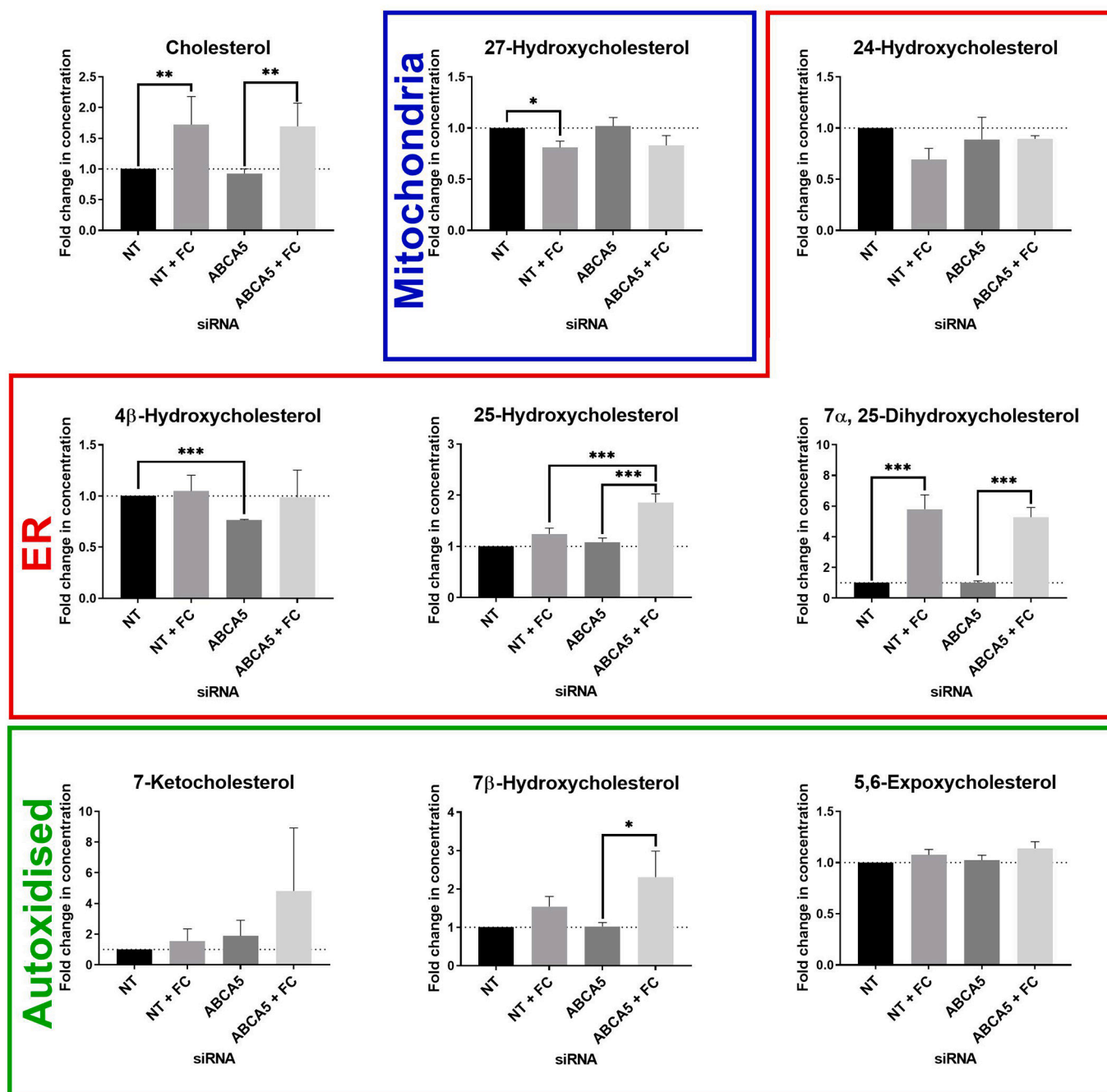

Fig. 8. Lipidomic analysis of free cholesterol-loaded outer root sheath keratinocytes with ABCA5 knockdown. Mass spectrometry analysis of ORS keratinocytes transfected with siRNA for 48 h and subsequently exposed to 25 μM FC or 0.5 % ethanol vehicle control for 24 h. Blue box donates mitochondrial derived oxysterols, red box for ER derived oxysterols and green box for autoxidised oxysterols. Data are mean ± SEM of N = 6 donors, except for 4β-hydroxycholesterol, 7α,25-hydroxycholesterol, 5,6-epoxycholesterol (N = 4) and 24-hydroxycholesterol (N = 2). One-way ANOVA or Kruskal Wallis tests were performed; significance denoted by * P ≤ 0.05, *** P ≤ 0.005.

reduction in the transcription of HMGCR was shown (Fig. 7I, K). This could be explained in terms of the reduction in SREBP2 transcriptional activity (Fig. 7M).

3.6. Sterol profile in free cholesterol-loaded outer root sheath keratinocytes

Next lipidomic analysis was performed to determine whether ABCA5 knockdown impacted the sterol profile (FC and oxysterols) in ORS keratinocytes. Oxysterols are oxidised forms of cholesterol and known to cross membranes faster than cholesterol. Oxysterols can also activate transcription factors such as LXR and suppress SREBP2, and are an important component in the homeostatic control of cellular sterol status [50].

As shown with the filipin staining, lipidomic analysis demonstrated a significant increase in the concentration of cellular FC following FC treatment for 24 h; both in NT and ABCA5 knockdown ORS keratinocytes (Fig. 8). Concentrations of individual oxysterols are displayed in Table S1, with Fig. 8 showing the normalised fold change. The most abundant oxysterols were 27-hydroxycholesterol, 4β-hydroxycholesterol, 7-ketocholesterol and 7β-hydroxycholesterol.

7α, 25-Dihydroxycholesterol significantly increased with FC loading, and was not altered by ABCA5 knockdown. A significant increase was detected for 7β-hydroxycholesterol in ABCA5 siRNA-treated keratinocytes following exogenous FC loading, which did not occur in NT cells (Fig. 8). A significant increase in 25-hydroxycholesterol was observed in ABCA5 siRNA keratinocytes loaded with exogenous FC; this was significantly higher than that observed in FC loaded NT siRNA keratinocytes (Fig. 8). A significant reduction in 27-hydroxycholesterol was observed in NT-treated keratinocytes following loading with FC; the reduction in ABCA5 siRNA-treated cells did not reach the level of significance.

3.7. Ex vivo culture of hair follicles with ABCA5 siRNA promotes anagen

Loss of function mutations in ABCA5 have been reported in patients with congenital hypertrichosis [5–7]. In order to assess the function of ABCA5 in hair growth, *ex vivo* culture of human HFs with self-delivering siRNA was performed. HFs follow a cycle through periods of highly proliferative growth (anagen), apoptosis mediated regression (catagen) and relative quiescence (telogen). Results from a pilot study ($N = 1$ donor) indicated that knockdown of ABCA5 may promote hair growth through prolongation of anagen (Fig. S2). We therefore assessed the exposure of HFs to FC for 24 h following 72 h siRNA (Fig. 9), to determine the hair growth response to excess exogenous cholesterol.

Analysis of ABCA5 protein levels following knockdown revealed significant decreases in pixel intensity for both ABCA5 siRNA alone and HFs treated with FC. Whereas, addition of FC to NT-treated follicles resulted in an increase in ABCA5 protein expression (Fig. 9D). Analysis of HF lengths revealed a significant increase in growth and the number of anagen HFs with ABCA5 knockdown in comparison to control (Fig. 9B+C).

FC treated control HFs did not show any significant increases in proliferation, however a significant reduction in the number of TUNEL+ cells of the bulb was detected. ABCA5 knockdown resulted in a significant increase in the percentage of Ki67+ cells and decrease in TUNEL+ cells in the bulb and DP stalk (Fig. 9E, F). Both ABCA5 knockdown and treatment with FC alone increased the number of cells in the bulb and DP (Fig. 9G). No significant differences for TUNEL+ cells or cell numbers were detected in ABCA5 knockdown HFs when cultured with or without FC, however there was a significant decrease in proliferation in FC treated ABCA5 knockdown HFs, in comparison to ABCA5 knockdown alone (Fig. 9E). No changes in pigmentation were observed with Masson Fontana staining for any treatment group (Fig. 9H).

These results share similarities with non-transfected cultured HFs where neither FC nor methyl-β-cyclodextrin treatment altered

proliferation, apoptosis or pigmentation (Fig. S3+4).

4. Discussion

Here, we provide a deeper insight into the potential roles of ABCA5 in cholesterol transport and homeostasis in ORS keratinocytes. Using a physiologically relevant concentration of FC based on previous literature [51], we confirmed that ABCA5 protein localisation can be modulated by changes in cellular cholesterol levels, which also altered intracellular co-localisation to *endo*-lysosomes, ER and mitochondria. Using siRNA-mediated knockdown, ABCA5 was implicated in the maintenance of cholesterol homeostatic pathways. Furthermore, endo-lysosomal cholesterol trafficking was found to be influenced by ABCA5 levels.

Previously, we reported intracellular ABCA5 expression in the human HF, along with plasma membrane localisation specifically in the hair shaft cuticle [40]. It is possible that, like ABCA1 [52], ABCA5 shuttles between endo-lysosomes and the plasma membrane to modulate plasma membrane efflux of cholesterol. However, as ABCA5 knockdown was shown to reduce ABCA1 mRNA and protein abundance in our study, it could also be postulated that the reduction in ApoA1 stimulated efflux observed is a result of ABCA1 loss, rather than being caused by changes in ABCA5 functioning directly in plasma-membrane cholesterol efflux. In support of this, no change in cholesterol efflux to HDL was detected, which is also consistent with the lack of change in ABCG1 and SCARB1 expression, both of which utilise HDL as an acceptor for cholesterol efflux. Notably, this conflicts with data seen in mouse derived *Abca5*$^{-/-}$ macrophages, where the loss of cholesterol efflux to HDL and not ApoA1 was observed [53].

We have previously reported low-levels of ABCG1 expression in the HF when compared to both ABCA1 and ABCA5 [40]. This could indicate a lower capacity for ABCG1-mediated cholesterol efflux. Species-specific differences in cholesterol transport may also exist. The murine *Abca5*$^{-/-}$ model reported by Ye et al. [53] demonstrated increased Abca1 expression, whereas we report a reduction in ABCA1 following ABCA5 knockdown in human ORS keratinocytes. This may explain the differences in cholesterol efflux observed between the current study, and that reported by Ye et al. [53]. Furthermore, there is evidence of tissue-specific differences in the predominant routes for cholesterol transport, with divergent ABC transporter expression patterns described in peripheral tissues [1,54].

Knockdown of ABCA5 in ORS keratinocytes reveals a disruption in the regulatory pathways controlling cholesterol homeostasis. This includes the loss of *SRBEP2* gene expression and transcriptional activity, along with dysregulation of the normal homeostatic response of LXR target genes to excess cholesterol. As co-localisation of ABCA5 to intracellular organelles increases with cholesterol loading, ABCA5 may be an integral component of intracellular cholesterol movement. Thus, a loss of ABCA5 following siRNA treatment would be expected to impair cholesterol movement, altering both efflux pathways and the rate of oxysterol production. Increased levels of di-hydroxy oxysterol upon FC loading indicates that ORS keratinocytes upregulate cholesterol metabolism pathways to maintain cholesterol homeostasis *via* oxysterol efflux, to reduce the intracellular accumulation.

There is a notable lack of evidence for whether exogenous sources of cholesterol are involved with hair growth. Indeed, HFs express LDLR and SRB1 which suggest a capacity for the uptake exogenous sources of cholesterol from LDL and HDL, respectively. Moreover, whereas an association of high circulating cholesterol levels and AGA has been reported by numerous studies [55–68], no differences in the activity of the rate limiting enzyme of cholesterol biosynthesis, HMGCR, has been detected in hypercholesteraemic patients in comparison to healthy controls [69]. Additionally, cohort studies have indicated no direct relationship between the use of cholesterol lowering statins and hair loss [70]. As we also showed that the addition of FC or cholesterol depletion in *ex vivo* HF culture did not significantly alter hair growth, small
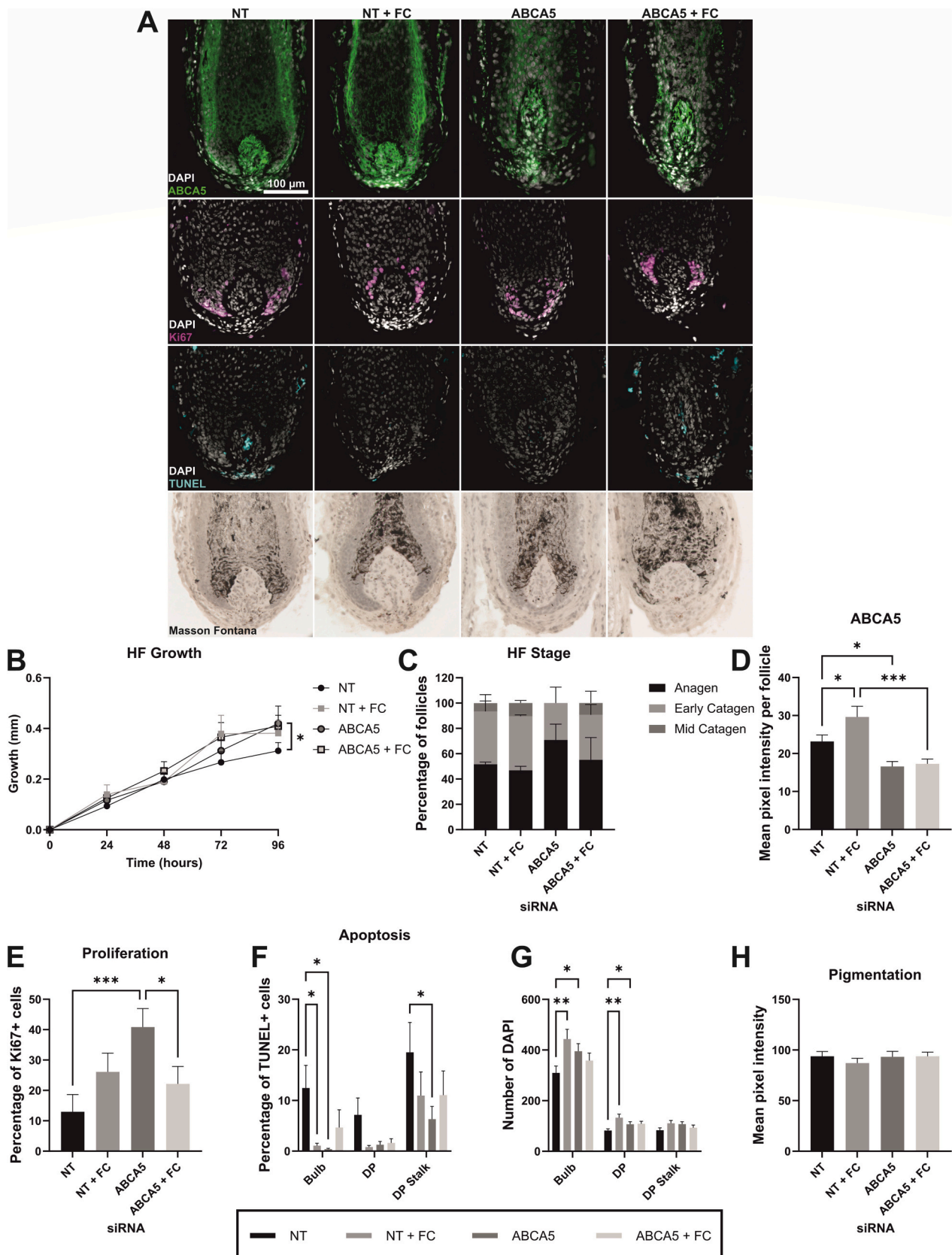
Fig. 9. *Ex vivo HF* culture with ABCA5 siRNA. (A) Immunofluorescence staining of ABCA5 (Green), Ki67 (Magenta) and TUNEL (cyan), along with Masson Fontana staining of *ex vivo* HFs transfected with NT or ABCA5 siRNA for 72 h followed by 25 μM FC for 24 h. Image analysis of (B) mean pixel intensity of ABCA5, (D) percentage of ki67+ cells below Auber's line, (F) percentage of TUNEL positive cells or (G) total nuclei in bulb, dermal papilla (DP) and DP stalk of hair follicle, (H) mean pixel intensity of Masson Fontana staining. (C) Percentage of HFs in anagen, early catagen and mid catagen (N = 2). (E) Hair follicle growth. Data are mean ± SEM for *n* = 26 follicles from N = 2 donors. One-way ANOVA tests were performed; significance denoted by * P ≤ 0.05, ** P ≤ 0.01, *** P ≤ 0.005.

changes in circulatory cholesterol levels are unlikely to influence hair loss.

Yet, loss of function mutations in ABCA5 have been observed in congenital hypertrichosis patients, and in line with this we report increased hair growth in ABCA5 knockdown HFs. Treatment of HFs with the LXR agonist T0901317 was reported to reduce hair growth *ex vivo* [71]; taken together with our data showing a reduction in the expression of LXR target genes in ABCA5 knockdown keratinocytes, this could suggest that the increase in hair growth observed following ABCA5 knockdown in cultured HFs, as well with patients with congenital hypertrichosis, may be caused by a reduction in LXR signalling.

Given the range of signalling molecules (*i.e.* Shh, Wnt/β-catenin, and the JAK/STAT pathway) known to influence HF morphogenesis, hair growth and hair cycling, with which cholesterol and its metabolites interact, there remain several additional possibilities that might explain how altered cholesterol homeostasis caused by ABCA5 deletion results in the excessive hair growth experienced by patients with congenital hypertrichosis. In brief, membrane lipids are important for the activation of Shh and Wnt/β-catenin signalling cascades [20,72], and binding of cholesterol to dishevelled is associated with activation of canonical over non- canonical Wnt signalling [73]. Inhibition of the JAK/STAT pathway has been shown to induce hair growth [74], and interactions of ABCA1 with APOA1 have been shown to activate the JAK/STAT pathway [75–77].

Here, we show that ABCA5 knockdown results in the dysregulation of cholesterol homeostasis, including a reduction in cholesterol efflux to ApoA1. These data suggest that ABCA5 plays a role in maintaining cellular cholesterol levels, with the potential for ABCA5 to function in intracellular cholesterol movement *via endo*-lysosomal transport. These data also provide some insight into the potential mechanisms for excessive hair growth in certain individuals. An ABCA5 loss-of-function mutation, and subsequent alterations in cholesterol homeostasis, have the potential to alter signalling pathways integral to the control of hair morphogenesis and growth, including Shh, Wnt/β-catenin or JAK/STAT. Further research into the roles played by both cholesterol and ABCA5 could help establish new avenues of investigation for treating disorders of hair growth.

CRediT authorship contribution statement

Megan A. Palmer: Formal analysis, Methodology, Writing – original draft, Visualization. **Irundika H.K. Dias:** Formal analysis, Resources, Investigation, Writing – review & editing. **Eleanor Smart:** Formal analysis, Resources, Investigation, Writing – review & editing. **Yvonne Benatzy:** Formal analysis, Investigation, Visualization. **Iain S. Haslam:** Conceptualization, Funding acquisition, Supervision, Writing – review & editing.

Declaration of competing interest

The authors declare that they have no known competing financial interests or personal relationships that could have appeared to influence the work reported in this paper.

Data availability

Data will be made available on request.

Acknowledgements

Appendix A. Supplementary data

Supplementary data to this article can be found online at https://doi.org/10.1016/j.bbalip.2023.159361.

References

[1] F. Quazi, R.S. Molday, Lipid transport by mammalian ABC proteins, Essays Biochem. 50 (2011) 265–290.

[2] Y. Fu, J.H. Hsiao, G. Paxinos, G.M. Halliday, W.S. Kim, ABCA5 regulates amyloid-beta peptide production and is associated with Alzheimer's disease neuropathology, J. Alzheimers Dis. 43 (2015) 857–869.

[3] D. Ye, I. Meurs, M. Ohigashi, L. Calpe-Berdiel, K.L.L. Habets, Y. Zhao, Y. Kubo, A. Yamaguchi, T.J.C. Van Berkel, T. Nishi, M. Van Eck, Macrophage ABCA5 deficiency influences cellular cholesterol efflux and increases susceptibility to atherosclerosis in female LDLr knockout mice, Biochem. Biophys. Res. Commun. 395 (2010) 387–394.

[4] Y. Kubo, S. Sekiya, M. Ohigashi, C. Takenaka, K. Tamura, S. Nada, T. Nishi, A. Yamamoto, A. Yamaguchi, ABCA5 resides in lysosomes, and ABCA5 knockout mice develop lysosomal disease-like symptoms, Mol. Cell. Biol. 25 (2005) 4138–4149.

[5] G.M. DeStefano, M. Kurban, K. Anyane-Yeboa, C. Dall'Armi, G. Di Paolo, H. Feenstra, N. Silverberg, L. Rohena, L.D. Lopez-Cepeda, V. Jobanputra, K.A. Fantauzzo, M. Kiuru, M. Tadin-Strapps, A. Sobrino, A. Vitebsky, D. Warburton, B. Levy, J.C. Salas-Alanis, A.M. Christiano, Mutations in the cholesterol transporter gene ABCA5 are associated with excessive hair overgrowth, PLoS Genet. 10 (2014), e1004333.

[6] R. Hayashi, K. Yoshida, R. Abe, H. Niizeki, Y. Shimomura, First Japanese case of congenital generalized hypertrichosis with a copy number variation on chromosome 17q24, J. Dermatol. Sci. 85 (2017) 63–65.

[7] R. Raza, A. Ullah, N. Haider, J. Krishin, M. Shah, F.U. Khan, T. Abdullah, S.I. Hansen, W. Raza, S. Basit Ahmad, Exome sequencing reveals the first intragenic deletion in ABCA5 underlying autosomal recessive hypertrichosis, Clin. Exp. Dermatol. (2022).

[8] K.R. Feingold, The outer frontier: the importance of lipid metabolism in the skin, J. Lipid Res. 50 (Suppl) (2009) S417–S422.

[9] P.W. Wertz, Lipids and barrier function of the skin, Acta Derm. Venereol. Suppl. (Stockh.) 208 (2000) 7–11.

[10] H. Tsuruoka, W. Khovidhunkit, B.E. Brown, J.W. Fluhr, P.M. Elias, K.R. Feingold, Scavenger receptor class B type I is expressed in cultured keratinocytes and epidermis. Regulation in response to changes in cholesterol homeostasis and barrier requirements, J. Biol. Chem. 277 (2002) 2916–2922.

[11] T. Inoue, Y. Miki, K. Abe, M. Hatori, M. Hosaka, Y. Kariya, S. Kakuo, T. Fujimura, A. Hachiya, S. Honma, S. Aiba, H. Sasano, Sex steroid synthesis in human skin in situ: the roles of aromatase and steroidogenic acute regulatory protein in the homeostasis of human skin, Mol. Cell. Endocrinol. 362 (2012) 19–28.

[12] D. Thiboutot, S. Jabara, J.M. McAllister, A. Sivarajah, K. Gilliland, Z. Cong, G. Clawson, Human skin is a steroidogenic tissue: steroidogenic enzymes and cofactors are expressed in epidermis, normal sebocytes, and an immortalized sebocyte cell line (SEB-1), J. Invest. Dermatol. 120 (2003) 905–914.

[13] K.U. Schallreuter, S. Hasse, H. Rokos, B. Chavan, M. Shalbaf, J.D. Spencer, J.M. Wood, Cholesterol regulates melanogenesis in human epidermal melanocytes and melanoma cells, Exp. Dermatol. 18 (2009) 680–688.

[14] Y.J. Jiang, P. Kim, P.M. Elias, K.R. Feingold, LXR and PPAR activators stimulate cholesterol sulfotransferase type 2 isoform 1b in human keratinocytes, J. Lipid Res. 46 (2005) 2657–2666.

[15] E.H. Epstein, M.L. Williams, P.M. Elias, The epidermal cholesterol sulfate cycle, J. Am. Acad. Dermatol. 10 (1984) 866–868.

[16] H.M. Elbadawy, F. Borthwick, C. Wright, P.E. Martin, A. Graham, Cytosolic StAR-related lipid transfer domain 4 (STARD4) protein influences keratinocyte lipid phenotype and differentiation status, Br. J. Dermatol. 164 (2011) 628–632.

[17] F. Spörl, M. Wunderskirchner, O. Ullrich, G. Bomke, U. Breitenbach, T. Blatt, H. Wenck, K.P. Wittern, A. Schrader, Real-time monitoring of membrane cholesterol reveals new insights into epidermal differentiation, J. Invest. Dermatol. 130 (2010) 1268–1278.

[18] P. Huang, D. Nedelcu, M. Watanabe, C. Jao, Y. Kim, J. Liu, A. Salic, Cellular cholesterol directly activates smoothened in hedgehog signaling, Cell 166 (2016) 1176–1187.e1114.

[19] J.Y. Tang, P.L. So, E.H. Epstein Jr., Novel hedgehog pathway targets against basal cell carcinoma, Toxicol. Appl. Pharmacol. 224 (2007) 257–264.

[20] J.P. Incardona, S. Eaton, Cholesterol in signal transduction, Curr. Opin. Cell Biol. 12 (2000) 193–203.

[21] C. Mathay, M. Pierre, M.R. Pittelkow, E. Depiereux, A.F. Nikkels, A. Colige, Y. Poumay, Transcriptional profiling after lipid raft disruption in keratinocytes identifies critical mediators of atopic dermatitis pathways, J. Invest. Dermatol. 131 (2011) 46–58.

[22] A. Slominski, B. Zbytek, G. Nikolakis, P.R. Manna, C. Skobowiat, M. Zmijewski, W. Li, Z. Janjetovic, A. Postlethwaite, C.C. Zouboulis, R.C. Tuckey, Steroidogenesis in the skin: implications for local immune functions, J. Steroid Biochem. Mol. Biol. 137 (2013) 107–123.

[23] E. Ikonen, Cellular cholesterol trafficking and compartmentalization, Nat. Rev. Mol. Cell Biol. 9 (2008) 125–138.

[24] W.J. Shen, S. Azhar, F.B. Kraemer, SR-B1: a unique multifunctional receptor for cholesterol influx and efflux, Annu. Rev. Physiol. 80 (2018) 95–116.

[25] I. Tabas, Consequences of cellular cholesterol accumulation: basic concepts and physiological implications, J. Clin. Invest. 110 (2002) 905–911.

[26] C.M. Adams, J. Reitz, J.K. De Brabander, J.D. Feramisco, L. Li, M.S. Brown, J. L. Goldstein, Cholesterol and 25-hydroxycholesterol inhibit activation of SREBPs by different mechanisms, both involving SCAP and Insigs, J. Biol. Chem. 279 (2004) 52772–52780.

[27] M.C. Phillips, Molecular mechanisms of cellular cholesterol efflux, J. Biol. Chem. 289 (2014) 24020–24029.

[28] M.A. Palmer, L. Blakeborough, M. Harries, I.S. Haslam, Cholesterol homeostasis: links to hair follicle biology and hair disorders, Exp. Dermatol. 29 (2020) 299–311.

[29] T. Aasen, J.C. Izpisua Belmonte, Isolation and cultivation of human keratinocytes from skin or plucked hair for the generation of induced pluripotent stem cells, Nat. Protoc. 5 (2010) 371–382.

[30] E. Bodo, T. Biro, A. Telek, G. Czifra, Z. Griger, B.I. Toth, A. Mescalchin, T. Ito, A. Bettermann, L. Kovacs, R. Paus, A hot new twist to hair biology: involvement of vanilloid receptor-1 (VR1/TRPV1) signaling in human hair growth control, Am. J. Pathol. 166 (2005) 985–998.

[31] I.S. Haslam, L. Jadkauskaite, I.L. Szabo, S. Staege, J. Hesebeck-Brinckmann, G. Jenkins, R.K. Bhogal, F.L. Lim, N. Farjo, B. Farjo, T. Biro, M. Schafer, R. Paus, Oxidative damage control in a human (mini-) organ: Nrf2 activation protects against oxidative stress-induced hair growth inhibition, J. Invest. Dermatol. 137 (2017) 295–304.

[32] A. Limat, F.K. Noser, Serial cultivation of single keratinocytes from the outer root sheath of human scalp hair follicles, J. Invest. Dermatol. 87 (1986) 485–488.

[33] E.A. Langan, M.P. Philpott, J.E. Kloepper, R. Paus, Human hair follicle organ culture: theory, application and perspectives, Exp. Dermatol. 24 (2015) 903–911.

[34] M. Philpott, M.R. Green, T. Kealey, Studies on the biochemistry and morphology of freshly isolated and maintained rat hair follicles, J. Cell Sci. 93 (Pt 3) (1989) 409–418.

[35] M.P. Philpott, Culture of the human pilosebaceous unit, hair follicle and sebaceous gland, Exp. Dermatol. 27 (2018) 571–577.

[36] J. Schindelin, I. Arganda-Carreras, E. Frise, V. Kaynig, M. Longair, T. Pietzsch, S. Preibisch, C. Rueden, S. Saalfeld, B. Schmid, J.-Y. Tinevez, D.J. White, V. Hartenstein, K. Eliceiri, P. Tomancak, A. Cardona, Fiji: an open-source platform for biological-image analysis, Nat. Methods 9 (2012) 676–682.

[37] S. Michelis, L. Danglot, R. Vauchelles, A.S. Klymchenko, M. Collot, Imaging and measuring vesicular acidification with a plasma membrane-targeted ratiometric pH probe, Anal. Chem. 94 (2022) 5996–6003.

[38] P. Bankhead, M.B. Loughrey, J.A. Fernández, Y. Dombrowski, D.G. McArt, P. D. Dunne, S. McQuaid, R.T. Gray, L.J. Murray, H.G. Coleman, J.A. James, M. Salto-Tellez, P.W. Hamilton, QuPath: open source software for digital pathology image analysis, Sci. Rep. 7 (2017) 16878.

[39] U. Schmidt, M. Weigert, C. Broaddus, G. Myers, Cell Detection with Star-convex Polygons, arXiv e-prints, (2018) arXiv:1806.03535.

[40] M.A. Palmer, E. Smart, I.S. Haslam, Localisation and regulation of cholesterol transporters in the human hair follicle: mapping changes across the hair cycle, Histochem. Cell Biol. 15 (2021) 529–545.

[41] A. Radhakrishnan, J.L. Goldstein, J.G. McDonald, M.S. Brown, Switch-like control of SREBP-2 transport triggered by small changes in ER cholesterol: a delicate balance, Cell Metab. 8 (2008) 512–521.

[42] D.I. Danylchuk, P.-H. Jouard, A.S. Klymchenko, Targeted solvatochromic fluorescent probes for imaging lipid order in organelles under oxidative and mechanical stress, J. Am. Chem. Soc. 143 (2021) 912–924.

[43] F. Ogasawara, F. Kano, M. Murata, Y. Kimura, N. Kioka, K. Ueda, Changes in the asymmetric distribution of cholesterol in the plasma membrane influence streptolysin O pore formation, Sci. Rep. 9 (2019) 4548.

[44] M. Holtta-Vuori, E. Sezgin, C. Eggeling, E. Ikonen, Use of BODIPY-cholesterol (TF-Chol) for visualizing lysosomal cholesterol accumulation, Traffic 17 (2016) 1054–1057.

[45] I.S. Haslam, C. El-Chami, H. Faruqi, A. Shahmalak, C.A. O'Neill, R. Paus, Differential expression and functionality of ATP-binding cassette transporters in the human hair follicle, Br. J. Dermatol. 172 (2015) 1562–1572.

[46] Y.J. Jiang, B. Lu, P. Kim, P.M. Elias, K.R. Feingold, Regulation of ABCA1 expression in human keratinocytes and murine epidermis, J. Lipid Res. 47 (2006) 2248–2258.

[47] Y.J. Jiang, B. Lu, E.J. Tarling, P. Kim, M.Q. Man, D. Crumrine, P.A. Edwards, P. M. Elias, K.R. Feingold, Regulation of ABCG1 expression in human keratinocytes and murine epidermis, J. Lipid Res. 51 (2010) 3185–3195.

[48] N. Wang, L. Yvan-Charvet, D. Lutjohann, M. Mulder, T. Vanmierlo, T.W. Kim, A. R. Tall, ATP-binding cassette transporters G1 and G4 mediate cholesterol and desmosterol efflux to HDL and regulate sterol accumulation in the brain, FASEB J. 22 (2008) 1073–1082.

[49] N. Wang, D.L. Silver, P. Costet, A.R. Tall, Specific binding of ApoA-I, enhanced cholesterol efflux, and altered plasma membrane morphology in cells expressing ABC1, J. Biol. Chem. 275 (2000) 33053–33058.

[50] V.M. Olkkonen, O. Beaslas, E. Nissila, Oxysterols and their cellular effectors, Biomolecules 2 (2012) 76–103.

[51] H. Shiigi, H. Matsumoto, I. Ota, T. Nagaoka, Detection of skin cholesterol by a molecularly imprinted electrode, Journal of Flow Injection Analysis 25 (2008) 81.

[52] E.B. Neufeld, A.T. Remaley, S.J. Demosky, J.A. Stonik, A.M. Cooney, M. Comly, N. K. Dwyer, M. Zhang, J. Blanchette-Mackie, S. Santamarina-Fojo, H.B. Brewer Jr., Cellular localization and trafficking of the human ABCA1 transporter, J. Biol. Chem. 276 (2001) 27584–27590.

[53] D. Ye, I. Meurs, M. Ohigashi, L. Calpe-Berdiel, K.L. Habets, Y. Zhao, Y. Kubo, A. Yamaguchi, T.J. Van Berkel, T. Nishi, M. Van Eck, Macrophage ABCA5 deficiency influences cellular cholesterol efflux and increases susceptibility to atherosclerosis in female LDLr knockout mice, Biochem. Biophys. Res. Commun. 395 (2010) 387–394.

[54] L. Zhou, C. Li, L. Gao, A. Wang, High-density lipoprotein synthesis and metabolism (review), Mol. Med. Report. 12 (2015) 4015–4021.

[55] S. Arias-Santiago, M.T. Gutierrez-Salmeron, A. Buendia-Eisman, M.S. Giron-Prieto, R. Naranjo-Sintes, A comparative study of dyslipidaemia in men and woman with androgenic alopecia, Acta Derm. Venereol. 90 (2010) 485–487.

[56] J.A. Ellis, M. Stebbing, S.B. Harrap, Male pattern baldness is not associated with established cardiovascular risk factors in the general population, Clin. Sci. (Lond.) 100 (2001) 401–404.

[57] C.A. Guzzo, D.J. Margolis, J. Johnson, Lipid profiles, alopecia, and coronary disease: any relationship? Dermatol. Surg. 22 (1996) 481.

[58] S. Sasmaz, M. Senol, A. Ozcan, G. Dogan, C. Tuncer, O. Akyol, S. Sener, The risk of coronary heart disease in men with androgenetic alopecia, J. Eur. Acad. Dermatol. Venereol. 12 (1999) 123–125.

[59] K.H. Sharma, A. Jindal, Association between androgenetic alopecia and coronary artery disease in young male patients, Int J Trichology 6 (2014) 5–7.

[60] M. Trevisan, E. Farinaro, V. Krogh, F. Jossa, D. Giumetti, G. Fusco, S. Panico, C. Mellone, S. Frascatore, A. Scottoni, et al., Baldness and coronary heart disease risk factors, J. Clin. Epidemiol. 46 (1993) 1213–1218.

[61] F. Acibucu, M. Kayatas, F. Candan, The association of insulin resistance and metabolic syndrome in early androgenetic alopecia, Singap. Med. J. 51 (2010) 931–936.

[62] N.F. Agamia, T. Abou Youssif, A. El-Hadidy, A. El-Abd, Benign prostatic hyperplasia, metabolic syndrome and androgenic alopecia: is there a possible relationship?, Arab, J. Urol. 14 (2016) 157–162.

[63] H.S. Banger, S.K. Malhotra, S. Singh, M. Mahajan, Is early onset androgenic alopecia a marker of metabolic syndrome and carotid artery atherosclerosis in young Indian male patients? Int J Trichology 7 (2015) 141–147.

[64] S. Chakrabarty, R. Hariharan, D. Gowda, H. Suresh, Association of premature androgenetic alopecia and metabolic syndrome in a young Indian population, Int J Trichology 6 (2014) 50–53.

[65] S. Arias-Santiago, M.T. Gutierrez-Salmeron, A. Buendia-Eisman, M.S. Giron-Prieto, R. Naranjo-Sintes, Lipid levels in women with androgenetic alopecia, Int. J. Dermatol. 49 (2010) 1340–1342.

[66] S. Arias-Santiago, M.T. Gutierrez-Salmeron, L. Castellote-Caballero, A. Buendia-Eisman, R. Naranjo-Sintes, Male androgenetic alopecia and cardiovascular risk factors: a case-control study, Actas Dermosifiliogr. 101 (2010) 248–256.

[67] S. Arias-Santiago, M.T. Gutierrez-Salmeron, L. Castellote-Caballero, A. Buendia-Eisman, R. Naranjo-Sintes, Androgenetic alopecia and cardiovascular risk factors in men and women: a comparative study, J. Am. Acad. Dermatol. 63 (2010) 420–429.

[68] O.A. Bakry, S.M. El Farargy, N. Ghanayem, A. Soliman, Atherogenic index of plasma in non-obese women with androgenetic alopecia, Int. J. Dermatol. 54 (2015) e339–e344.

[69] P.G. Brannan, J.L. Goldstein, M.S. Brown, 3-hydroxy-3-methylglutaryl coenzyme A reductase activity in human hair roots, J. Lipid Res. 16 (1975) 7–11.

[70] L. Smeeth, I. Douglas, A.J. Hall, R. Hubbard, S. Evans, Effect of statins on a wide range of health outcomes: a cohort study validated by comparison with randomized trials, Br. J. Clin. Pharmacol. 67 (2009) 99–109.

[71] L.E. Russell, W.J. Harrison, A.W. Bahta, C.C. Zouboulis, J.M. Burrin, M.P. Philpott, Characterization of liver X receptor expression and function in human skin and the pilosebaceous unit, Exp. Dermatol. 16 (2007) 844–852.

[72] K.S. Stenn, P. Karnik, Lipids to the top of hair biology, J. Invest. Dermatol. 130 (2010) 1205–1207.

[73] R. Sheng, H. Kim, H. Lee, Y. Xin, Y. Chen, W. Tian, Y. Cui, J.-C. Choi, J. Doh, J.-K. Han, W. Cho, Cholesterol selectively activates canonical Wnt signalling over non-canonical Wnt signalling, Nat. Commun. 5 (2014) 4393.

[74] S. Harel, C.A. Higgins, J.E. Cerise, Z. Dai, J.C. Chen, R. Clynes, A.M. Christiano, Pharmacologic inhibition of JAK-STAT signaling promotes hair growth, Sci. Adv. 1 (2015), e1500973.

[75] M.J. Kim, Y.J. Lee, Y.S. Yoon, M. Kim, J.H. Choi, H.S. Kim, J.L. Kang, Apoptotic cells trigger the ABCA1/STAT6 pathway leading to PPAR-gamma expression and activation in macrophages, J. Leukoc. Biol. 103 (2018) 885–895.

[76] C. Tang, Y. Liu, P.S. Kessler, A.M. Vaughan, J.F. Oram, The macrophage cholesterol exporter ABCA1 functions as an anti-inflammatory receptor, J. Biol. Chem. 284 (2009) 32336–32343.

[77] G.J. Zhao, K. Yin, Y.C. Fu, C.K. Tang, The interaction of ApoA-I and ABCA1 triggers signal transduction pathways to mediate efflux of cellular lipids, Mol. Med. 18 (2012) 149–158.